

Emission Line Formation in a Relativistic Accretion Disk

GEORGE B. RYBICKI AND BENJAMIN C. BROMLEY

Harvard-Smithsonian Center for Astrophysics

ABSTRACT

The observed profile of spectral lines from a relativistic accretion disk can constrain parameters such as the disk geometry and the rotation of the central black hole. The formation of the spectral line in a disk generally has been modeled with simple assumptions such as local isotropy of emission. Here we consider line formation in the presence of velocity gradients induced by the differential flow in the disk. In this case the emission can have anisotropy in the form of an azimuthal dependence relative to the local principle axes of shear. Since the physical conditions in a disk are uncertain in detail, we investigate this effect with simple parameterized models based on Sobolev theory to highlight the overall character of the changes in the line profile. We find that velocity gradients generally cause a relative increase of flux in the red wing, hence the inner radius of the disk would be underestimated if the effect were not taken into consideration. If the inner radius is used as a signature of black hole rotation, as when the disk is not emissive within the marginally stable circular orbit, then the inferred rotation would be overestimated in cases where the emissivity of the disk has fairly shallow fall-off with radius. If the disk were emissive even within the marginally stable orbit, then the local azimuthal anisotropy of emission produces features in the line profile which distinguish rotating from nonrotating black holes.

Subject headings: accretion, accretion disks – black hole physics – galaxies: active – line: profiles

1 Introduction

The treatment of line formation in disks is dependent on a number of physical uncertainties and can be complicated if the medium is optically thick in the line. One complication is the presence of velocity gradients within the disk, which can affect the optical depth along a ray. A larger velocity gradient implies a smaller total optical depth because the same line absorption is spread out over a larger bandwidth. These velocity gradients are highly anisotropic: for example, the local gradient of line of sight velocity vanishes in a thin disk for rays which propagate radially outward from the disk or which are tangential to the Keplerian velocity field. The gradient reaches its maximum absolute value for rays at 45 degrees to the radial or tangential direction (see Rybicki & Hummer 1983). This implies that the emission along the radial and tangential directions are suppressed relative to that along the 45 degree directions. This can radically change the observed profile of the line, since it is the tangential rays that may contribute most strongly to the extreme Doppler shifts of the line.

For the case of nonrelativistic disks, these velocity gradient effects have usually been treated through use of the *Sobolev approximation*, which assumes that the velocity gradients are “large,” in the sense that the typical Doppler shift of the line due to velocity gradients is large compared with the intrinsic line width. Rybicki & Hummer (1983) discussed the validity of the Sobolev approximation for nonrelativistic thin accretion disks. Here the critical question is whether the vertical scale of the relevant line formation region is large enough for a single oblique ray to probe parts of the disk with substantially different velocities, i.e., different enough to shift the profile through its own width. Rybicki & Hummer (1983) concluded that the Sobolev approximation could be marginally applicable for disks where the scale of line formation was comparable to the entire disk thickness, but might be inapplicable when the relevant line formation region was confined to a much thinner layer near the top of the disk. In their treatment of nonrelativistic disks in cataclysmic variables, Horne & Marsh (1986) avoided making the Sobolev approximation of large velocity gradients to find the escape probabilities, but their results were still limited by the use of the escape probability method.

The effect of velocity gradients does not seem to have been previously considered for extreme relativistic disks around Schwarzschild or Kerr black holes. Instead, these treatments in essence assume that the emission

from each disk element is isotropic, both in local emission angle relative to the local disk normal and in local azimuthal angle.

It is the purpose of this paper to evaluate the potential effects of velocity gradients in the disk on the observed line profiles from relativistic disks. Because the detailed inclusion of these effects depend on knowledge of many as yet unknown physical properties of the disks, the development here can at most be a qualitative indication of the types of phenomena to be expected. We therefore find it instructive to model the azimuthal dependence of the emergent emission simply with the leading of a Fourier series as well as with the full prediction of Sobolev theory. This will allow us to make some useful statements about the range of effects on the observed line profiles due to velocity gradients and how such effects might be degenerate with the effects of black hole rotation.

2 The Line Formation Problem

In this section we review and extend the analytic theory of line formation in differentially rotating disks. In §2.1 we show how the observed line can be related to the intensity field emerging from each local element of the disk, including general relativistic effects. In §2.2 we discuss the line formation problem in the disk, using the Sobolev theory.

This will be followed by the discussion of several approximation schemes, including the general escape probability method and the Sobolev (large velocity gradient) escape probability method. Finally, these approximations are compared with some accurate numerical solutions.

2.1 The Specific Luminosity

Here we review and extend a number of results on the calculation of the line spectrum from accretion disks. Our notation will follow that of Rybicki (1970) and Rybicki & Hummer (1978, hereafter RH). The purpose is to find formulas for the observed monochromatic flux F_ν from a distant source (here, the accretion disk). We limit the discussion to the case where the source subtends a very small solid angle as viewed by the observer.

It is convenient to introduce the concept of the *specific luminosity* $\mathcal{L}_\nu(\mathbf{n})$ of the source, which is defined as the emitted energy at frequency ν per unit time, per unit frequency, and per unit solid angle in the direction \mathbf{n} of the observer. In Euclidean space, the monochromatic flux F_ν seen by the observer at large distance D is related to the specific luminosity by

$$F_\nu = D^{-2} \mathcal{L}_\nu(\mathbf{n}), \quad (1)$$

We remark that if the source is at cosmological distances, the observed flux can still be related to the specific luminosity, but now through the more general formula,

$$F_\nu = (1+z) D_L^{-2} \mathcal{L}_{\nu(1+z)}(\mathbf{n}), \quad (2)$$

where z is the redshift and D_L is the luminosity distance of the source.

The calculation of \mathcal{L}_ν can be facilitated by constructing an observer's *plane of the sky* at the source location, which is normal to the direction \mathbf{n} of the observed radiation. The specific luminosity can be expressed as an integral of the specific intensity $I_\nu(\mathbf{n})$ in direction \mathbf{n} over this plane of the sky,

$$\mathcal{L}_\nu(\mathbf{n}) = \int I_\nu(\mathbf{n}) dA. \quad (3)$$

The plane of the sky does not have to be right at the object, but should be sufficiently near so that both the object and the plane are essentially at the same distance from the observer.

For the non-relativistic case, the specific intensity field appearing in the surface integral equation (3) can be found by tracing back along each ray in a straight line until it intersects the disk, and by using the invariance of specific intensity along rays. This means that the intensity appearing in Eq. equation (3) is just equal to the corresponding intensity field emergent from the disk.

Both equations (1) and (3) can be directly applied to relativistic disks, i.e., those surrounding black holes or other compact objects for which general relativistic effects are significant, providing that the plane of the sky is chosen to be sufficiently far outside the gravitational field of the source (ideally at infinity, but in practice typically at hundreds of Schwarzschild radii). However, new complications arise in relating the

specific intensity field on the plane of the sky to the field emerging from the disk. Two effects must be taken into account: first, the rays now travel on curved paths in the strong gravitational field of the source, and second, the invariant quantity along rays is I_ν/ν^3 , not I_ν itself. These two effects can be expressed by introducing the specific intensity $I'_{\nu'}$, emergent from the disk corresponding to a particular ray in direction \mathbf{n} in the plane of the sky. We define the redshift factor g at each point of the plane of the sky to be the ratio of the frequency ν to the Doppler/gravitational shifted frequency ν' of the photon back along the same ray as viewed in the comoving frame of the disk, that is,

$$g = \frac{\nu}{\nu'} . \quad (4)$$

The transformation of specific intensity is then,

$$I_\nu = (\nu/\nu')^3 I'_{\nu'} = g^3 I'_{\nu'/g} . \quad (5)$$

Therefore the generalization of equation (3) to relativistic disks is,

$$\mathcal{L}_\nu(\mathbf{n}) = \int g^3 I'_{\nu'/g} dA . \quad (6)$$

The emergent specific intensity $I'_{\nu'}$, must be found from the physics of the accretion disk itself. For a thin disk, the radiation field depends on only a fairly small patch of the disk, for which it has been typical to use a locally nonrelativistic model as an approximation.

Emergent line radiation in the comoving frame of the disk is centered at the lab frequency of the line, which we shall denote ν_0 . The line width is typically much smaller than the magnitude of the subsequent frequency shifts due to Doppler/gravitation, so that it is a good approximation to write

$$I'_{\nu'} = \tilde{I} \delta(\nu' - \nu_0) , \quad (7)$$

where \tilde{I} is the integrated emergent line intensity in the comoving frame of the disk,

$$\tilde{I} = \int I'_{\nu'} d\nu' . \quad (8)$$

From well known transformation properties of δ -functions we have

$$I'_{\nu'/g} = g \tilde{I} \delta(\nu - g\nu_0) . \quad (9)$$

Using this in equation (6), we obtain

$$\mathcal{L}_\nu(\mathbf{n}) = \int g^4 \tilde{I} \delta(\nu - g\nu_0) dA . \quad (10)$$

An equivalent form of this equation was given by Chen, Halpern & Filippenko (1989).

Two alternative forms of equation (10) will now be given. The first is derived by introducing the level curves of the g -function in the plane of the sky. Let l be the arc length variable along each such level curve. The element of area can be written

$$dA = dl dw , \quad (11)$$

where dw is the width of the region between level curves corresponding to g and $g + dg$. It is clear that

$$dw = |\nabla g|^{-1} dg, \quad dA = |\nabla g|^{-1} dg dl . \quad (12)$$

The delta function in equation (10) may be expressed as

$$\delta(\nu - g\nu_0) = \nu_0^{-1} \delta(g - \nu/\nu_0) . \quad (13)$$

The integral of this delta function over g then leads to a formula for $\mathcal{L}_\nu(\mathbf{n})$ as a line integral,

$$\mathcal{L}_\nu(\mathbf{n}) = \nu_0^{-1} g^4 \int \tilde{I} |\nabla g|^{-1} dl \quad (14)$$

over the curve of constant g corresponding to $g = \nu/\nu_0$. (This curve might in general have several disconnected branches.)

We now derive a second alternative form for equation (10) that is more convenient for practical calculations. Let us introduce a discrete frequency grid and define averages of $\mathcal{L}_\nu(\mathbf{n})$ over frequency widths $\Delta\nu$ by

$$\tilde{\mathcal{L}}_\nu(\mathbf{n}) = \frac{1}{\Delta\nu} \int_{\nu - \frac{\Delta\nu}{2}}^{\nu + \frac{\Delta\nu}{2}} \mathcal{L}_{\nu'} d\nu' = \frac{1}{\Delta\nu} \int g^4 \tilde{I} B\left(\frac{\nu - g\nu'}{\Delta\nu}\right) dA \quad (15)$$

where $B(x)$ is the ‘‘boxcar’’ function

$$B(x) = \begin{cases} 1, & \text{if } |x| \leq \frac{1}{2}, \\ 0, & \text{otherwise.} \end{cases} \quad (16)$$

Replacing the integral by a sum over area elements ΔA_{ij} , we have,

$$\tilde{\mathcal{L}}_\nu(\mathbf{n}) = \frac{1}{\Delta\nu} \sum g_{ij}^4 \tilde{I}_{ij} B\left(\frac{\nu - g_{ij}\nu'}{\Delta\nu}\right) \Delta A_{ij} \quad (17)$$

To a consistent order of approximation, the factor g_{ij}^4 can be taken outside the summation and replaced by $(\nu/\nu_0)^4$. The boxcar function acts as a constraint on the summation, which leads to our second alternative expression for the specific luminosity,

$$\tilde{\mathcal{L}}_\nu(\mathbf{n}) = \frac{1}{\Delta\nu} \left(\frac{\nu}{\nu_0}\right)^4 \sum_{|\nu - g_{ij}\nu_0| \leq \frac{1}{2}\Delta\nu} \tilde{I}_{ij} \Delta A_{ij}. \quad (18)$$

This form is well suited to calculating $\tilde{\mathcal{L}}_\nu(\mathbf{n})$ by accumulating contributions in separate bins corresponding to the discrete frequency grid of resolution $\Delta\nu$.

In terms of algorithms for estimation of line profiles, equation (18) suggests the following: a pixel image of the source, as seen by distant observer, can be constructed wherein the pixels correspond to the area elements ΔA_{ij} . A calculation of the emergent intensity and frequency shift of the radiation detected at each pixel then enables the sum in equation (18) to be performed trivially. In practice, of course, one iterates over pixels in the observer’s sky plane and simply accumulates the specific luminosity in each frequency bin. The difficulty in this procedure is modeling an image of the source, which may involve relativistic effects such as gravitational lensing. However, ray-tracing codes — photon trajectory integrators — handle curved spacetime with facility if not always with efficiency. They are of use not only in determining the mapping of an observed pixel onto the source but can also help in the calculation of the frequency shift g , which depends on the 4-momenta of the emitted photons and the 4-velocity of the source element. We discuss these issues in the next section. But first we must consider a second possible complication, that of evaluating the local emergent intensity. We do so in the context of Sobolev theory.

2.2 Emergent Intensity and the Sobolev Approximation

The problem has now been reduced to determining the emergent integrated intensities \tilde{I} from the disk in a frame comoving with the disk material. Unfortunately, no definitive calculation of the emergent intensities is possible at this time, since it depends on highly uncertain disk parameters and even basic disk physics. Therefore one is forced to make a number of simplifying assumptions and approximations. We shall base our discussion on the Sobolev escape probability formalism.

Most of the work on relativistic disks has assumed that the emergent integrated intensity is some simple function of radial coordinate r , perhaps with some dependence on the emergent polar angle θ_{em} relative to the local disk normal (sometimes called the ‘‘limb-darkening law’’). The usual argument for the emergent intensity to depend only the polar angle θ_{em} and not on the azimuthal direction, is that each local patch of the disk is essentially plane-parallel, with complete azimuthal symmetry. However, from other work on accretion disks (see, e.g., Rybicki & Hummer 1983) it is known that line emission can be strongly influenced by local velocity gradients due to shear in the disk, and this can induce azimuthal dependence in the emergent intensities by causing frequency shifts in the line profiles of the same order or larger than the line widths.

We first review the calculation for the simple case of a nonrelativistic, Keplerian disk which is optically thin in the continuum but with arbitrary optical thickness in the line. (More details can be found in 1983.) The usual cylindrical coordinate system, r, φ, z will be used. The differential rotation of the disk will be, by assumption, constant on cylinders with angular velocity $\omega(r) \propto r^{-3/2}$, and the only nonzero components of the rate of strain tensor e_{ij} are $e_{r\phi_{\text{em}}} = e_{\phi_{\text{em}}r} = (1/2)r\omega' = (3/2)\omega$. Here the local azimuthal angle ϕ_{em} is measured with respect to the tangential velocity direction. The velocity gradient along the ray Q is given by

$$Q = \frac{3}{4}\omega \sin^2 \theta_{\text{em}} \sin 2\phi_{\text{em}} . \quad (19)$$

The emergent integrated intensity \tilde{I} can be expressed as the integral along the ray of the integrated emissivity ϵ times the escape probability P_{esc} ,

$$\tilde{I} = \int \epsilon(r, z) P_{\text{esc}}(r, z, \theta_{\text{em}}, \phi_{\text{em}}) dl . \quad (20)$$

Assuming that the quantities inside the integral depend only weakly on r , then this integral can be converted to one over the vertical direction,

$$\tilde{I} = \sec \theta_{\text{em}} \int \epsilon(r, z) P_{\text{esc}}(r, z, \theta_{\text{em}}, \phi_{\text{em}}) dz . \quad (21)$$

in which r appears only parametrically.

In the special case of an optically thin line, the escape probability is unity and we have

$$\tilde{I} = \sec \theta_{\text{em}} \int \epsilon(r, z) dz . \quad (22)$$

Thus the optically thin case shows strong ‘‘limb-brightening,’’ (the emergent radiation is more intense for grazing emergence than for normal emergence), but there is no dependence on the azimuthal angle ϕ_{em} for this case.

The opposite case is for a line that is optically thick at least up to some height $|z| = L$ from the disk midplane. For $|z| > L$ we assume that the region rapidly becomes optically thin in the line and does not contribute significantly to the emission. The escape probability in optically thick cases can be complicated by global transfer effects, and even the formula equation (20) may not be immediately useful because the emissivity itself may depend on the global transfer problem. However, for the case of large velocity gradients, it turns out that the transfer is quite local, and the theory is considerably simplified. The line optical thickness is given by the Sobolev optical depth

$$\tau_{\text{S}} = \frac{\kappa}{v_{\text{th}}|Q|} . \quad (23)$$

where κ is the integrated line opacity, and v_{th} is the thermal Doppler velocity of the emitting ion. The escape probability for optically thick line is to a good approximation given in terms of the Sobolev optical depth by the simple formula,

$$P_{\text{esc}} = \frac{1}{\tau_{\text{S}}} . \quad (24)$$

The emergent integrated intensity is then found by combining Eqs. 21, 23, and 24,

$$\tilde{I} = |Q| \sec \theta_{\text{em}} \int_{-L}^L S v_{\text{th}}^{-1} dz , \quad (25)$$

where $S = \epsilon/\kappa$ is the line source function. To apply this theory to thin relativistic disks, one must interpret Q to be c times the gradient of the redshift factor along the ray.

For the non-relativistic Keplerian disk, $|Q|$ may be replaced by equation (19), which gives

$$\tilde{I} = \frac{3}{4}\omega \sec \theta_{\text{em}} \sin^2 \theta_{\text{em}} |\sin 2\phi_{\text{em}}| \int_{-L}^L S v_{\text{th}}^{-1} dz . \quad (26)$$

Thus the angular distribution of the emitted line radiation at a particular patch of the disk is proportional to $\sec \theta_{\text{em}} \sin^2 \theta_{\text{em}} |\sin 2\phi_{\text{em}}|$. Although this result has been derived under a set of rather special assumptions, it

clearly demonstrates the potentially strong dependence of the emission on the azimuthal angle ϕ_{em} , through the factor $|\sin 2\phi_{\text{em}}|$. This factor vanishes for the radial and tangential directions (for which the line-of-sight velocity gradient vanishes), and is maximum for the $\phi_{\text{em}} = \pm 45^\circ$ lines.

Technically, the Sobolev approximation breaks down when the line-of-sight velocity gradient becomes small, so it is not strictly true that the emergent intensity actually vanishes for radial and tangential rays, but it is clear that the intensity will be reduced relative to the lines where $|\sin 2\phi_{\text{em}}| = 1$. For this reason, and because of other physical uncertainties in the theory, we shall parameterize the azimuthal dependence of the emergent integrated intensity using a Fourier cosine series with the same symmetry as $|\sin 2\phi_{\text{em}}|$,

$$\tilde{I} = \tilde{I}_0 \sec \theta_{\text{em}} + \tilde{I}_1 \sec \theta_{\text{em}} \sin_{\text{em}}^2 \theta \sum_{n=0}^{\infty} a_n \cos(4n\phi_{\text{em}}) \quad (27)$$

where the first term on the righthand side corresponds the emissivity of the disk in the absence of velocity gradient effects. To illustrate the effect that velocity gradients can have on emission line profiles, we will take consider an emergent intensity constructed with a gradient-free form and a first-order ‘‘correction’’ for azimuthal dependence given by the $n = 1$ term. Note that we recover equation (26) by setting $\tilde{I}_0 = 0$ and

$$a_n = \begin{cases} \frac{4n}{\pi(1-4n^2)} & n \neq 0 ; \\ 0 & n = 0 . \end{cases} \quad (28)$$

The Sobolev approximation breaks down when line-of-sight velocity gradients are small, since the local thermal broadening allows some line photons to escape even along paths of zero velocity gradient. This occurs in the present situation for a small set of emission angles near the zero-gradient directions. Although our Sobolev calculations are technically wrong at these angles, we expect that the overall solution will not be too much affected. Our first order angular expansion method errs in the opposite sense by giving too much emission along those directions, and indicates that the zero-gradient problem does not affect our general conclusions.

In order to evaluate the effect of small velocity gradients properly, other, more exact, treatments of line formation should be used. Such a treatment for a nonrelativistic accretion disk was presented by Horne & Marsh (1986), who found the total emergent intensity without use of the Sobolev approximation. They were able to carry out most of the calculation analytically by making several simplifying assumptions about the structure of the disk, such as isothermal vertical structure and constant line source function. The resulting model of emergent intensity has parameters which include a degenerate combination of the height and temperature of the disk: the height regulates the breadth of line emission from the range of Doppler shifts along a given line of sight, while the temperature governs the intrinsic breadth of the line at any given point in the disk. The ratio of these line breadths determines the extent to which velocity gradients can affect the emergent intensity — the limit of zero temperature is the domain of the Sobolev approximation.

Making analogous assumptions about the vertical structure and the temperature as a function of position in the disk, it would be straightforward to evaluate the emergent flux with a modified Horne & Marsh model. However, the purpose of the present work is to estimate the importance of the effect of velocity gradients in relativistic disks where the run of temperature is not well-constrained, and the Sobolev theory and the first-order correction term in equation (27) seem better suited to this preliminary analysis. We expect that our parameterization will at least qualitatively reproduce the effects of velocity gradients given by more detailed models, which we leave for future investigations.

3 Relativistic Considerations

In this section we consider aspects of line formation which are specific to relativistic thin accretion disks. We consider cases where disk material is in stable circular orbit (Keplerian in a relativistic sense), or, if any material exists within the marginally stable circular orbit at radius R_{ms} , it is assumed to be in freefall onto the black hole, with energy and angular momentum corresponding to the marginally stable orbit (see Cunningham 1975; also Reynolds & Begelman 1997). All material, whether in circular orbit or in freefall, is taken to lie in a slab whose thickness is everywhere small compared to the distance to the black hole. If the black hole itself has non-zero angular momentum then we assume that the disk is in the equatorial plane. This last assumption is justified by the Bardeen-Petterson (1975) effect which causes a viscous disk to stabilize in the equatorial plane of the rotating hole. With these specifications for the relativistic accretion disk system we proceed to calculate quantities relevant to line formation.

3.1 Ray Tracing

As described in §2.1, the calculation of a line profile may amount to generating an image of the source, and binning up the image's pixels according to frequency, weighted by pixel area, emergent intensity, and the fourth power of the frequency shift. We can impose some model for the emissivity over the face of the disk and apply corrections to the emergent intensity, I , if limb darkening or velocity gradients are present. What remains in the calculation is the mapping of the observer's pixels to the source, the frequency shift, and local emission angles upon which I may depend. A ray tracing code can provide the map from pixel to source, and its output, photon 4-momenta, can be used in conjunction with a model for the 4-velocity field of the source to obtain both g and local emission angles.

Here, we obtain pixel images of relativistic thin disks from the code described by Bromley, Chen & Miller (1997). It is a general-purpose geodesic solver which has an incarnation as a ray tracer when given photon positions and momenta on input. The code integrates photon trajectories back in time from a distant observers' sky plane until the photon intersects the disk. This is standard procedure for ray tracing since we always know where the desired photon trajectories end up (at the pixel array) but we may have only guesses as to where these trajectories might originate. Note that mapping from the source to the observer's sky plane is reasonable even in geometrically flat spaces. The case of image rotation is an example; if we map pixels in a source image to a (rotated) target image we may end up with target pixels which never receive a photon. This is never a problem if we map from image to source.

An output image of our code includes a list of pixels, their coordinates in the observer's sky plane, and the location and 4-momentum of the photons at the point of intersection with the disk.

As is standard in the literature, we work in Boyer-Lindquist coordinates, (t, r, θ, ϕ) , wherein the metric about a Kerr black hole of mass M and specific angular momentum a takes the form

$$ds^2 = -\chi^2 dt^2 + \Psi^2 (d\phi^2 - \omega dt)^2 + \frac{\rho^2}{\Delta} dr^2 + \rho^2 d\theta^2 \quad (29)$$

with

$$\begin{aligned} \chi^2 &= \frac{\Delta \rho^2}{A}, \quad \Psi^2 = \frac{A \sin^2 \theta}{\rho^2}, \\ A &= (r^2 + a^2)^2 - a^2 \Delta \sin^2 \theta, \quad \Delta = r^2 + a^2 - 2Mr, \\ \rho^2 &= r^2 + a^2 \cos^2 \theta, \quad \text{and} \quad \omega = \frac{2Mra}{A}. \end{aligned} \quad (30)$$

The contravariant 4-momentum of a photon with unit energy then becomes (Kojima 1991)

$$(p_t, p_r, p_\theta, p_\phi) = (-1, \pm\sqrt{R}/\Delta, \pm\sqrt{\Theta}, \lambda), \quad (31)$$

where

$$R = (r^2 + a^2 - \lambda)^2 - \Delta[(\lambda - a)^2 + \eta], \quad (32)$$

and

$$\Theta = \eta^2 + \cos^2 \theta \left(a^2 - \frac{\lambda^2}{\sin^2 \theta} \right). \quad (33)$$

The constants of motion, η and λ , along with location (r, θ, ϕ) of the photon at some point in time, fully specify the trajectory.

The photon coordinate energy in a local material frame follows from projecting the 4-momentum \vec{p} onto the material 4-velocity \vec{v} (the time basis vector of the material frame). The relative frequency of a photon exchanged between arbitrary material frames is thus

$$g \equiv \frac{-\vec{p}_{\text{rec}} \cdot \vec{v}_{\text{rec}}}{-\vec{p}_{\text{em}} \cdot \vec{v}_{\text{em}}}, \quad (34)$$

where the subscripts distinguish emitter and receiver of the photon. For the distant observer at rest with respect to the black hole we set the receiver 4-velocity to

$$\vec{v}_{\text{rec}} = \partial_t. \quad (35)$$

The 4-velocity of the emitter depends on the nature of mass flow in the disk. In a Keplerian disk, we find

$$\vec{u}_{\text{em}} = \frac{\gamma_{\text{kep}}}{\chi} (\partial_t + \Omega_{\text{kep}} \partial_\phi), \quad (36)$$

where

$$\Omega_{\text{kep}} = M^{1/2} / \left(r^{3/2} + M^{1/2} a \right) \quad (37)$$

is the coordinate angular velocity of a circular orbit and γ_{kep} is the Lorentz factor of the orbit with speed

$$\beta_{\text{kep}} = \frac{\Psi}{\chi} (\Omega_{\text{kep}} - \omega) \quad (38)$$

as measured in the locally nonrotating frame defined by Bardeen, Press & Teukolsky (1972; see also Novikov & Thorne 1973). The relative frequency of a photon from the disk detected by a distant observer is thus

$$g = \frac{1}{\chi \gamma_{\text{kep}} (1 - \Omega_{\text{kep}} \lambda)}. \quad (39)$$

The case of a non-Keplerian disk, where the emitters are in freefall from the minimum stable circular orbit has been considered by Cunningham (1975; details may be found in the appendix therein).

The local emission angles, expressed in spherical polar coordinates, come from projecting \vec{p}_{em} onto the spatial basis vectors in the local emitter frame:

$$\cos \theta_{\text{em}} = -\frac{\vec{p}_{\text{em}} \cdot \vec{e}_{\hat{\theta}}}{\vec{p}_{\text{em}} \cdot \vec{v}_{\text{em}}}, \quad \sin \theta_{\text{em}} \cos \phi_{\text{em}} = -\frac{\vec{p}_{\text{em}} \cdot \vec{e}_{\hat{r}}}{\vec{p}_{\text{em}} \cdot \vec{v}_{\text{em}}}, \quad \sin \theta_{\text{em}} \sin \phi_{\text{em}} = -\frac{\vec{p}_{\text{em}} \cdot \vec{e}_{\hat{\phi}}}{\vec{p}_{\text{em}} \cdot \vec{v}_{\text{em}}}. \quad (40)$$

Note that θ_{em} gives the local inclination angle of the photon trajectory relative to the disk surface, while ϕ_{em} is the angle between the photon's projected path in the disk plane and the line tangent to circular orbit. A value of $\phi_{\text{em}} = 0$ indicates emission in the forward direction of the material orbit.

In the Keplerian case, for example, the vectors in equations (40) are

$$\begin{aligned} \vec{e}_r &= \frac{\Delta^{1/2}}{r} \partial'_r, & \vec{e}_\theta &= \frac{1}{r} \partial_\theta, \\ \vec{e}_\phi &= \gamma_{\text{kep}} \left(\frac{\beta}{\chi} \partial_t + \frac{\Psi + \beta_{\text{kep}} \chi \omega}{\chi \Psi} \partial_\phi \right). \end{aligned} \quad (41)$$

3.2 Local Velocity Gradients

As discussed by RH and reviewed in §2.2, the optical depth in an emission line becomes large when the local emission angle is aligned with a constant-velocity surface. In the case of a nonrelativistic, thin disk, these surfaces appear as cross-hairs, “+”, with one hair parallel to the direction of flow in the Keplerian velocity field. When we proceed to the relativistic case, the constant velocity surface must be generalized to a surface of constant frequency shift so as to take into account effects of space-time curvature in addition to Doppler shifts.

We can map out the surfaces of constant frequency shift with a ray tracing technique, simply tracking photons from an emitter and noting the value of g at a spray of neighboring points. This can be performed with equation (34) which gives the observed frequency shift for any arbitrary emitter–receiver pair. In a Keplerian disk,

$$g = \frac{\chi(r) \gamma_{\text{kep}}(r + \Delta r) [1 - \Omega_{\text{kep}}(r + \Delta r) \lambda]}{\chi(r + \Delta r) \gamma_{\text{kep}}(r) [1 - \Omega_{\text{kep}}(r) \lambda]}, \quad (42)$$

where the emitter is located at (r, ϕ) and the receiver is at radius $(r + \Delta r, \phi + \Delta \phi)$. Note that the constant of motion λ is related to $\Delta \phi$. The constant-frequency surfaces then can be mapped out in the Boyer-Lindquist coordinates by varying λ and Δr .

It is useful to consider the problem of mapping the observed frequency shift evaluated at some small proper radius ϵ in the emitter frame as a function of emission angle. For now we consider only receiver locations which lie in the disk plane, but our conclusions will apply for disks with finite thickness as long as the velocity field is independent of altitude above the disk. A prescription is to choose λ , thereby fixing the photon 4-momentum (eq. [31]). This in turn sets the local emission angles, i.e., a unit vector along the photon propagation path as expressed in terms of the orthonormal basis of the emitter frame. We can then step to the point a distance ϵ away along this vector to evaluate the observed frequency shift g . To gauge the dependence of g on local emission angle ϕ_{em} in the small- ϵ limit, we may rewrite the photon 4-momentum

and 4-velocity at the receiver in terms of a Taylor expansion in r about the radial coordinate of the source. Then,

$$\begin{aligned} g &= \frac{(\vec{p} + \Delta r \vec{p}^{(r)}) \cdot (\vec{v} + \Delta r \vec{v}^{(r)})}{\vec{p} \cdot \vec{v}}, \\ &= 1 + \frac{\vec{p} \cdot \Delta r \vec{v}^{(r)}}{\vec{p} \cdot \vec{v}} + \frac{\Delta r \vec{p}^{(r)} \cdot \vec{v}}{\vec{p} \cdot \vec{v}} + O(\Delta r^2), \end{aligned} \quad (43)$$

where all 4-vectors are evaluated at r and the superscript denotes differentiation with respect to r . Evidently the second term on the RHS of equation (43) is a Doppler term, since $\Delta r \vec{v}^{(r)}$ represents a change in the velocity field, while the third term is associated with gravitational redshifting of the photon. In the case of a Keplerian disk, the third term vanishes because the gravitational redshift gradient is orthogonal to the velocity flow. Then, since $\Delta r \sim \sin \phi_{\text{em}}$ and $\vec{p} \cdot \vec{v}^{(r)} \sim \cos \phi_{\text{em}}$, we recover the nonrelativistic result in the limit of small ϵ :

$$g - 1 \sim \sin 2\phi_{\text{em}}. \quad (44)$$

Deviations from this expression for finite ϵ cause distortions in the sine-wave dependence of g on local emission angle, but the zero-crossings, and hence the constant-frequency-shift surfaces, are preserved.

For the case of freefall orbits, similar results can be obtained although in this case there are convergent flow lines and changes in velocity along the direction of flow. Numerical calculations nonetheless confirm that the cross-hair form for the zero-frequency-shift surfaces is a reasonable approximation.

4 Results: Line Profile Calculations

We have reviewed all the ingredients necessary to estimate the effects of velocity gradients on emission line profiles from relativistic accretion disks. Thus armed we proceed to numerically calculate profiles in the following three settings: 1) a stable Keplerian disk with an inner radius at the marginally stable limit, $R_{m.s} = 6 R_g$ around a Schwarzschild black hole ($R_g = \sqrt{GM/c^2}$ is the gravitational radius of the black hole); 2) a stable Keplerian disk extending down to $1.25 R_g$ around an extreme Kerr black hole; and 3) a disk in freefall inside marginally stable orbit around a Schwarzschild hole. In all of these cases we take the intrinsic disk emissivity \tilde{I}_0 (see eq. [27]) to be a power law in radius with index α in the range of -4 to 0. Throughout we seek the changes that velocity gradients can cause in a line profile and we wish to determine how these changes can affect the interpretation of the profile if they are not taken into account. Specifically we are interested to know if these effects cause confusion or highlight the differences between profiles of the three systems listed above.

We begin with an illustration (Fig. 1) of the dependence of a line profile on the choice of power-law index α . For the moment we only consider Keplerian disks. By definition, steeper power laws enhance emission of the inner disk. Note that in the Schwarzschild system, with the Keplerian disk extending down to its innermost stable orbit, the location of the blue peak must be above $\nu/\nu_e = 0.72$ for any inclination angle i ; this limit rises with increasing i , so that at $i = 30^\circ$, the blue peak is located above 0.92, regardless of α . The trough between the two peaks of the Schwarzschild case is a characteristic of this system. The trough can be “filled in” to some degree by weighting outer disk components more strongly, although the result is always to create a stronger blue peak close to the rest frame frequency of the line. In contrast, the line profiles observed from a disk around an extreme Kerr black hole can have a much shallower trough from emission of sources below $6 R_g$ (e.g., Laor 1991). This property provides a signature of the Kerr system in addition to the extended red wing (e.g., Laor 1991). However, the signature is strong only if the inner disk component is heavily weighted, with $\alpha \lesssim -2$.

Changes in the line profile from variation of other parameters, namely the inclination angle and disk radii, have been considered in the literature (Asaoka 1989; Laor 1991; Kojima 1991; Bromley, Chen & Miller 1997). In qualitative terms, an increasing inclination angle broadens the line profile and tends to strengthen the signatures of emission at small disk radii. The latter effect comes from the increased importance of gravitational amplification at high inclination angle. In a Schwarzschild system, when $\alpha \gtrsim -4$ and the radial extent of the disk is finite, two Doppler peaks are generally evident in the line profiles; the red peak directly reflects the outer disk radius and the inclination angle while the precise location of the blue peak depends on the index α as well as the inclination angle and disk radii. Kerr systems are similar except that distinct

Doppler peaks may no longer exist because the blue peaks from emitters at small radii can be redder than the red peaks from sources at large radii.

The simple power-law emissivity model just described is built on the assumption that the sources in a disk are isotropic in their rest frames, and that their distribution on a given disk annulus is uniform. The latter assumption is relaxed in studies of emission from “hot spots” on the disk (e.g., Bao 1992). The isotropy assumption has also been relaxed for relativistic accretion disks, but only in the context of limb darkening, that is, a dependence on the emission angle θ_{em} . In the present study, we consider the dependence on azimuthal emission angle ϕ_{em} to determine how velocity gradients might affect a disk line and if they can cause confusion in the interpretation of a line as coming from a Schwarzschild or Kerr system. The details of radiative transfer are uncertain, inasmuch as the physical structure of an accretion disk around a supermassive black hole has yet to be determined. Thus, as promised, we use only the highest amplitude ($n = 1$) term in the expansion for emergent flux given in equation (27). We hereafter refer to this term as the “leading correction” for velocity gradients.

Figure 2 shows the effect of the leading correction to the line profile from a Schwarzschild system. Evidently, the trough in the Schwarzschild profile is enhanced after the velocity-gradient effect is included. A similar enhancement is seen in the extreme Kerr system (Fig. 3). To neglect the velocity-gradient effect, if it indeed is present in an observed emission line, is to overestimate the depth of the central trough. Thus, confusion between Kerr and Schwarzschild systems may result.

This point is illustrated in Figure 4 wherein profiles with and without velocity-gradient corrections are superimposed. If the data are noisy at the level of recent ASCA observations (e.g., Tanaka et al. 1995), then certain key features of a Kerr system such as emission from small radii will not be directly detected. The form of the line profile above $\nu/\nu_e \sim 0.6$, in particular the depth of the trough between red and blue peaks, is thus crucial to the identification of a Kerr system. In Figure 4 profiles from a Schwarzschild system in which the velocity gradient is important are compared with profiles from Kerr and Schwarzschild systems in which the effect is irrelevant. As illustrated, profiles from a corrected Schwarzschild system may be misinterpreted as evidence of an extreme Kerr model on the basis of a χ^2 metric. However, the confusion can only occur if the emissivity index is near -2 or greater, so that the inner Kerr disk is not weighted heavily.

It is evident from Figures 1–4 that if one interprets a line profile as having a non-disk Gaussian component (e.g., Iwasawa et al. 1996), then the excess blue peak caused by the velocity gradient correction will no longer be associated with the disk line and its removal will cause the profile to more closely resemble a Kerr system.

In the case of a freefalling disk in a Schwarzschild system significantly redshifted emission may be comparable to that seen in the extreme Kerr case with a Keplerian disk. All orbits are unstable, as they are assumed to be infinitesimally perturbed inward from R_{ms} at $6 R_g$. Reynolds & Begelman (1997) imply that the line profiles from a freefalling disk and a Kerr system may be indistinguishable and we confirm that result (see Fig. 5). Evidently the differences in orbital trajectories make only negligible changes in the observed photon redshifts, at least when integrated over the disk. However, if the local emission angles play a role, as in the velocity gradient effect, then the trajectory differences become important. Figure 5 illustrates that in some instances when the inner disk, the velocity gradient effect can break the approximate degeneracy in the profile shapes.

5 Summary

We have reviewed aspects of the line formation problem for a relativistic accretion disk. Our new contribution is to include the effects of velocity gradients on line luminosity when the disk has some optical thickness in the line. From the illustrations given in the previous section we can draw the following conclusions regarding the use of line profiles to determine properties of the accretion disk/black hole system from the shape of line profiles. If disks are stable, then the velocity-gradient effect can mimic an increase in the emission from small radii. When the inner disk is not too heavily weighted, for example if emissivity index is -2 or more, then black hole rotation might be spuriously inferred. If disks are emissive even in freefall, then the effects of rotation are virtually invisible in the line profiles. However, in this case the velocity-gradient effect may help distinguish the Kerr and Schwarzschild systems, as it can leave a different imprint on otherwise similar profiles. This is possible only if the inner disk is weighted heavily, as when the emissivity index is less than -2.

The velocity gradient effect may have relevance to the iron $K\alpha$ emission lines which have been recently studied (e.g., Tanaka et al. 1995) in data from Seyfert 1 galaxies. The $K\alpha$ line complex arises primarily from

fluorescence. If an accretion disk is cold, with material less ionized than Fe XVIII, then it will be optically thin in the line and no velocity gradient effect will be observable. However, the effect might occur in the inner region of the disk which may support higher ionization states that will resonantly scatter emission line photons. Thus the effect may be measurable, offering a new probe of the local environment of the central supermassive black hole.

This work was supported by NSF grant PHY 95-07695. The Cray supercomputer used in this research was provided through funding from the NASA Offices of Space Sciences, Aeronautics, and Mission to Planet Earth.

REFERENCES

- Asaoka, I., 1989, PASJ, 41, 76
Bardeen, J. M. & Petterson, J. A. 1975, ApJ Lett., 195, L65
Bardeen, J. M., Press, W. H., & Teukolsky, S. A. 1972, ApJ, 178, 347
Bromley, B. C., Chen, K., & Miller, W. A. 1997, ApJ, 475, 57
Carter, B. 1968, Phys. Rev., 174, 1559
Chen, K., Halpern, J.P., & Filippenko, A.V. 1989, ApJ, 339, 742
Cunningham, C. T., 1975, ApJ, 202, 788
Dabrowski, Y., Fabian, A. C., Iwasawa, K., Lasenby, A. N., & Reynolds, C. S. 1997 preprint (astro-ph/9704177)
Horne, K., & Marsh, T.R. 1986, MNRAS, 218,761
Iwasawa, K., et al. 1996, MNRAS, 282, 1038
Karas, V., Vokrouhlický, D., & Polnarev, A. G. 1992, MNRAS, 259, 569
Kojima, Y. 1991, MNRAS, 250, 629
Laor, A. 1991, ApJ, 376, 90
Nandra, K., George, I. M., Mushotzky, R. F., Turner, T. J., & Yaqoob, T. 1997, ApJ, 476, 70
Novikov, I. D., & Thorne, K. S. 1973, in Black Holes, C. DeWitt & B. DeWitt, eds. (New York: Gordon Breach).
Reynolds, C. S., & Begelman, M. C. 1997, ApJ, in press (astro-ph/9705136).
Reynolds, C. S., Fabian, A. C., Nandra, K., Inoue, H., Kunieda, H., & Iwasawa, K. 1995, MNRAS, 277, 901
Rybicki, G.B. 1970, *Spectrum Formation in Stars with Steady-state Extended Atmospheres*, Eds. Groth, H.G., & Wellman, P., NBS special publication 332, p. 87
Rybicki, G.B., & Hummer, D.G. 1978, ApJ, 219, 654
Rybicki, G. B., & Hummer, D. G. 1983, ApJ, 274, 380
Speith, R., Riffert, H., & Ruder, H. 1995, Comp. Phys. Comm., 88, 109
Tanaka, Y. et al. 1995, Nature, 352, 659

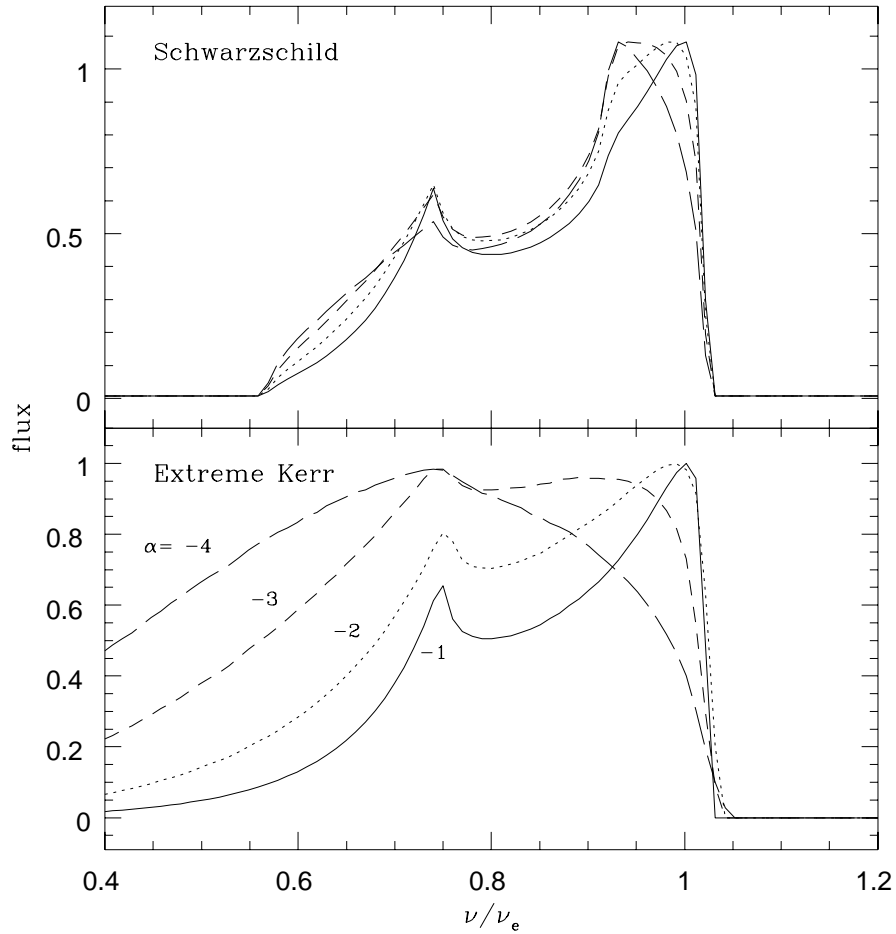


Fig. 1.— Line profiles from disk models with locally isotropic, power-law emissivity functions for various values of the index α . The upper plot corresponds to a Keplerian disk of radii between $6 R_g$ and $12 R_g$ around a nonrotating black hole. The lower plot corresponds to a Keplerian disk about a Kerr black hole with extremal angular momentum; the inner and outer radii of the disk are $1.25 R_g$ and $12 R_g$. The inclination angle in both cases is 30° .

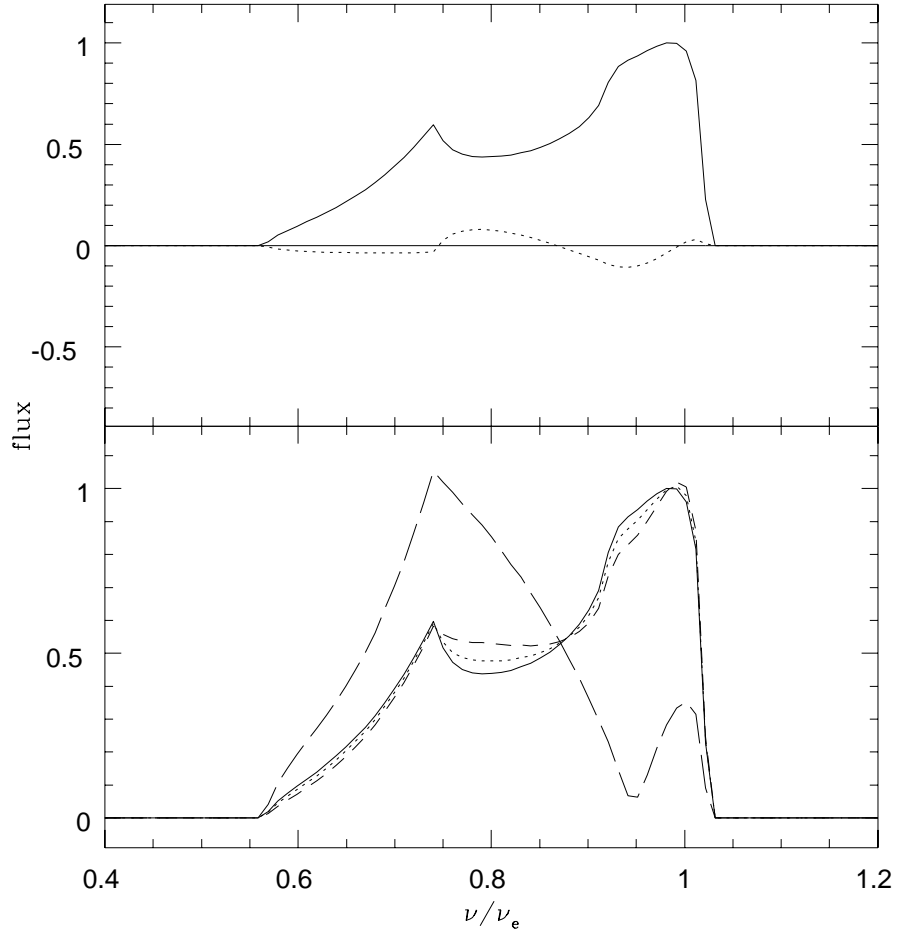


Fig. 2.— Line profiles from a Schwarzschild disk model with a power-law emissivity index $\alpha = -2$. Inclination angle and disk radii are the same as in Figure 1. The upper plot shows the case of isotropic emission (solid curve) and the flux contribution (dotted line) from the first-order correction for the velocity gradient effect. The lower plot shows the isotropic case and linear combinations with the first-order contribution. The weights of the first-order terms are 0.3 (dotted curve) and 0.5 (short dashed curve). The prediction of the Sobolev theory is show as well (long dashed cyrve).

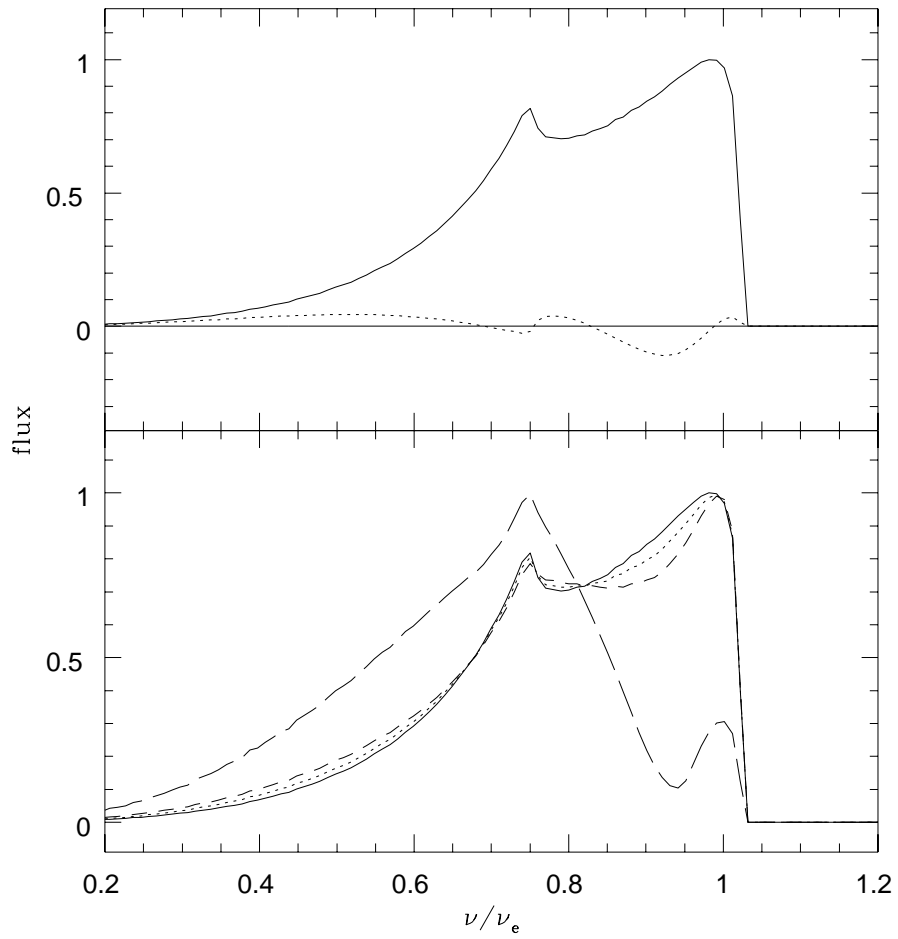


Fig. 3.—: Same as Figure 2 except for a Kerr disk with inner radius of $1.25 R_g$.

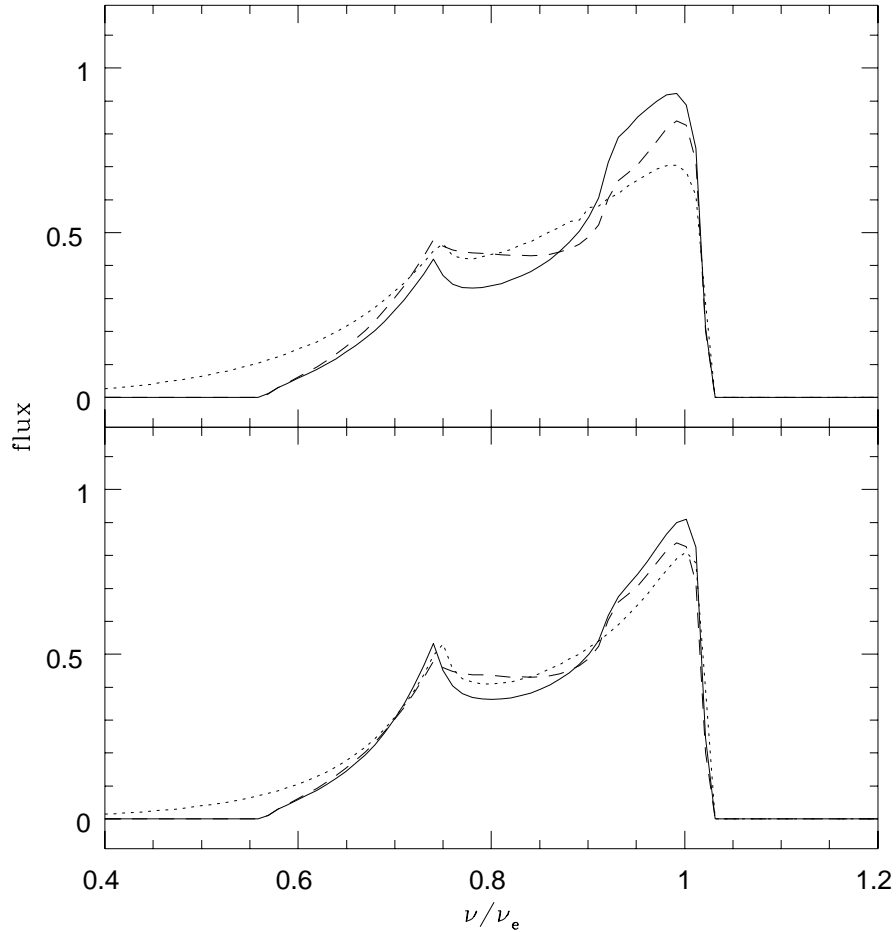


Fig. 4.— Comparison of line profiles with and without first-order velocity gradient corrections. The upper plot shows profiles from both Schwarzschild (solid curve) and Kerr (dotted curve) systems with $\alpha = -2$ and the same disk parameters as in Figure 1. A profile from the Schwarzschild system, corrected for the velocity gradient effect to first order with limb-darkening factor of $\sin(\theta_e)$, is also shown (dashed curve). In the lower plot, the same corrected profile is shown, but now superimposed on profiles from Schwarzschild and Kerr systems with $\alpha = -1$.

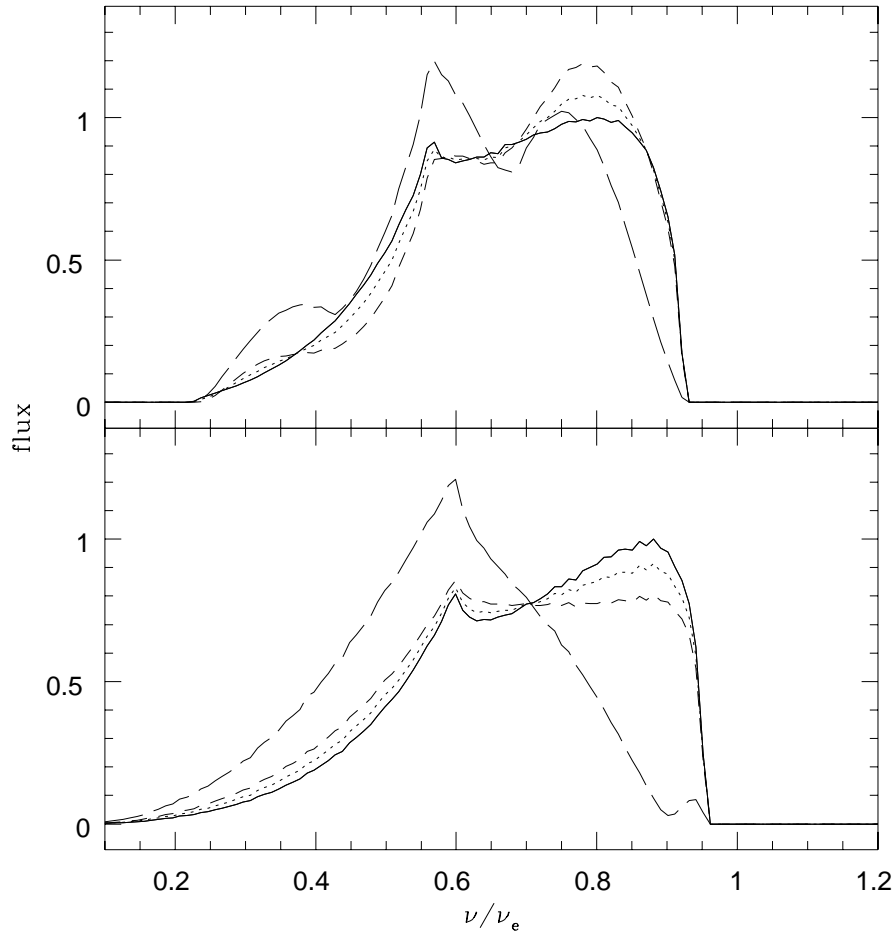


Fig. 5.— Line profiles from disk material below $6 R_g$. The upper plot is for a disk in freefall from the marginally stable orbit down to a radius of $2.1 R_g$ about a nonrotating black hole. The lower plot corresponds to a disk around an extreme Kerr hole with an inner radius of $1.25 R_g$. In both cases the inclination angle is 30° and the emissivity index is -2 . The curves indicate different levels of contribution from the velocity-gradient effect, as in Figure 2.